Numerical algorithms for capillary electrophoresis

Sergey V. Ermakov☆ Michael S. Bello☆☆ and Pier Giorgio Righetti*

Faculty of Pharmacy and Department of Biomedical Sciences and Technologies University of Milano, Via Celoria 2, Milan 20133 (Italy)

ABSTRACT

Three groups of algorithms applied to mass transport equations in electrokinetic processes are described and compared. They are used for solving a set of partial differential equations expressing the conservation of mass and charge laws, the dissociation equilibria and electroneutrality. These equations should be able to predict the shape and structure of the boundaries and peak diffusion and anomalies as the analytes are driven in the electric field past the detector port. Three different numerical algorithms have been proposed: by Mosher *et al.* (*The Dynamics of Electrophoresis*, VCH, Weinheim, 1992), by Dose and Guiochon [*Anal. Chem.*, 63 (1991) 1063–1072] and by Ermakov *et al.* [*Electrophoresis*, 13 (1992) 838–848]. The first two algorithms offer numerical solutions which can only be implemented at unrealistically low current densities, two to three orders of magnitude lower than normally adopted in practical electrophoresis. When applied to real experimental conditions, both previous algorithms break down: the separated analyte zones, as obtained by simulation, decay into several solitary waves (solitons), resulting from the action of numerical dispersion. In contrast, the numerical algorithms proposed by Ermakov *et al.* still allow the prediction of peaks of with the correct shape, with only minor non-physical spikes.

INTRODUCTION

Progress in theoretical studies of electrophoresis processes nowadays depend more and more on computer simulations, because only with the help of a computer can one move forward in solving the set of numerical non-linear electrophoresis equations. Only a few simplified limiting cases of these equations could be solved analytically. The alterative to an analytical solution for complex equations is a numerical solution with the help of a computer which allows one to model a practical process governed by non-linear partial differential equations (PDEs). Computer simulations are able to help an ex-

perimenter to investigate the effects of the ion mobilities, pH and other parameters on the results of the separation run and/or to optimize the analysis conditions.

In the field of electrophoresis, numerical modelling was commenced by Bier's group about 10 years ago. An extensive review of what has been done since then with relevant references can be found in a recently published book by Mosher *et al.* [1]. Previous work demonstrated that all types of electrophoresis are governed by the same set of PDEs expressing the conservation laws of mass and charge, dissociation equilibria and electroneutrality. Examples of modelling give good qualitative agreement with experiments for different modes of electrophoresis.

Nevertheless, there is still a gap between numerical modelling and experiments. In order to bridge the gap and make numerical modelling a useful tool for a practitioner (as it is in fluid dynamics, heat transfer and some other fields), one has to be convinced that the results of

---

* Corresponding author.
☆ Permanent address: Keldysh Institute of Applied Mathematics, Russian Academy of Sciences, Miusskaya Sq. 4, Moscow 125047, Russian Federation.
☆☆ Permanent address: Institute of Macromolecular Compounds, Russian Academy of Sciences, Bolshoi 31, St. Petersburg 199004, Russian Federation.

modelling are in agreement with those given by real experiments. Today, most of the papers dealing with numerical solutions of electrophoresis equations present solely calculated concentration, pH and conductivity profiles *along the column axis* or, in the best case, compare them with *time dependences* of a UV sensor signal. Hence quantitative comparison of the experimental and calculated results is impossible and, usually, is not the goal of such simulations. However, as has been pointed out in a review [2] of the book by Mosher *et al.* [1], "Quantitative evidence, *e.g.*, simulated and experimental results side by side with a graphical output format that uses the same coordinate system..." is desirable. We believe that the aforesaid describes not only what the particular book lacks but what the whole field of numerical modelling in electrophoresis is missing.

Numerical algorithms help only if they are very carefully elaborated and adjusted to the equations they are supposed to solve. This is well known in fluid mechanics where the development of new algorithms and numerical modelling has become a separate scientific field called "computational fluid dynamics". Electrophoresis equations are very similar to those of fluid dynamics and, therefore, most of the problems encountered there might be expected to appear in numerical simulations of electrophoresis processes. The main difficulty in a numerical solution of electrophoresis equations arises from a solution for the unsteady (*i.e.*, time-dependent) mass transport equations when they describe moving zones with sharp non-uniformities of concentrations, velocities, temperature, etc., similar to shock waves in gas dynamics.

There are several approaches for a numerical solution of electrophoresis equations based on finite-difference techniques [1,3–13]. All algorithms applied to the mass transport equations in electrophoresis simulations may be divided into three groups: that used in refs. 1 and 4–6, that used in refs. 3 and 7–10 and that used in refs. 13 and 14. The first two groups [1,3–10] use similar methods for representing space derivatives in the transport equation and differ mostly in the method of temporal discretization. The algorithms used there under certain circumstances

give solutions with spurious oscillations (see ref. 1, p. 58, and ref. 3). In order to avoid these oscillations and numerical instabilities, one is forced either to use high-speed computers [3] or to simulate separations at current densities more than two orders of magnitude less than experimental current densities [4]. In the first case these algorithms cannot be used on the personal computers usually provided with a capillary electrophoresis unit. In the second case, a prediction made for current densities two orders of magnitude less than those routinely adopted experimentally can hardly be interpreted as being quantitative.

In an attempt to improve numerical methods for unsteady electrophoresis equations, a high-resolution finite-difference algorithm based on a finite-difference scheme with artificial dispersion [11] has recently been developed by Ermakov *et al.* [12,13]. This algorithm was successfully applied to the simulation of capillary zone electrophoresis (CZE) and capillary isotachophoresis (ITP) [14], where it showed its ability to resolve sharp isotachophoretic boundaries and demonstrated excellent agreement with exact analytical results [15]. The algorithm [13] has been extended to multi-dimensional simulations, particularly to column electrophoresis, where two-dimensional sample evolution was studied [16].

This paper aims at testing and comparing the different numerical algorithms, particularly the properties of finite-difference schemes used for the solution of mass transport equations. All three numerical schemes, used for electrophoretic simulations, are implemented and applied to electrophoretic problems having explicit analytical solutions. This approach shows drawbacks inherent in specific numerical methods. Examples of simulations for CZE and ITP runs allow one to compare three numerical algorithms. The results of these numerical experiments exhibit limits of validities for these schemes and thus shed light on their applicability to real electrophoresis problems. The results of simulations are presented in the same form as seen by an experimenter, namely as dependences of concentration *versus* time for parameters of simulations corresponding to normal experimental conditions.

This is not the only approach we have adopted in bringing computer science into the realm of electrophoresis. In a recent development, Bello et al. [17] proposed a computer program able to predict buffer temperature and electric current in CZE as a function of capillary diameter, type of cooling device, buffer conductivity and applied voltage gradient. This program calculates with high precision the temperature inside the capillary, and can thus predict mobility shifts of analytes run with different voltage gradients. Given that today a number of CZE units are laboratory made and lack forced liquid cooling, this program should enable the experimenter to program precisely the temperature at which to perform a separation. This parameter is of utmost importance in, e.g., micellar electrokinetic chromatography (since the partition coefficient of the analyte is strongly temperature dependent) [18] and in DNA separations, for runs below or above the melting point of double-stranded DNAs [19]. In yet another approach, we have applied computer science to the optimization of pH gradients to be adopted in isoelectric focusing separations with insolubilized buffers and titrants [20]. This program, developed over a 10-year period [21], allows the modelling of linear and non-linear (convex and concave exponentials, sigmoidal) gradients utilizing mixtures of up to 50 buffers and titrants. Its use in single- and two-dimensional separations of protein mixtures is now routine and its use has been instrumental in novel findings in, e.g., molecular biology, biochemistry and human pathology [22]. This program is now being introduced into chromatographic science for separations performed under non-isocratic conditions.

THEORY

All modes of electrophoresis are governed by the general set of PDEs including mass transport equations for all components of the solution, the equation of charge conservation, the equation of electroneutrality and algebraic equations of ionic equilibria [1]. These equations form the basis for a general theoretical treatment of electrophoresis and the starting point for numerical simulations in particular. For the solution containing mono-valent weak acids and bases the equations are reported in Appendix A. Further, we restrict ourself to capillary electrophoresis and particularly to CZE and ITP. This section presents known analytical solutions for mass transport PDE, which are further used as reference patterns for comparing different numerical methods. Numerical methods for mass transport equations used for electrophoresis simulations are also described.

Analytical solutions to unsteady mass transport equations in electrophoresis

Only in a few limiting cases are analytical solutions for these equations known. Here we mention two of them for zone electrophoresis:

(1) Sample zones migrate with constant velocities determined by their electrophoretic mobilities and do not interact either with each other or with the buffer. The mass transport equation is linear and the well known solution in this instance for the sample introduced as an infinitely narrow band is the Gaussian peak migrating with constant velocity in the direction parallel to the direction of applied electric field, i.e., along the capillary axis.

(2) A sample zone changes the electric conductivity of the background electrolyte σ_0, but not its pH, and migrates without diffusion. The conductivity σ in the sample zone is linearly dependent on the concentration of the sample C according to $\sigma = \sigma_0(1 - \alpha C)$, where α is a proportionality coefficient. Both sample and buffer are uni–univalent electrolytes (see Refs. 23 and 24 and references cited therein). The analytical solution is a discontinuous function.

In both instances the concentration of the sample constituent is governed by the mass transport equation [23];

$$\frac{\partial C}{\partial t} + \frac{\partial (uC)}{\partial x} = D \cdot \frac{\partial^2 C}{\partial x^2} \qquad (1)$$

$$u = u_0/(1 - \alpha C) \qquad (2)$$

where u_0 is the migration velocity at the sample infinite dilution, x is the axis coordinate along the capillary, t is time and D is the diffusion coefficient.

The first case of a linear equation can be obtained from eqns. 1 and 2 by setting $\alpha = 0$ in eqn. 2, whereas the equation for the second case corresponds to $\alpha \neq 0$, $D = 0$.

It is convenient to take analytical solutions for eqn. 1 corresponding to particular forms of initial conditions: to the form of a Gaussian peak of unit height in the first case and to the form of a rectangular pulse of a height C_0 in the second case. The initial conditions are shown graphically in Fig. 1 and are represented by the following equations:

$$C(x, 0) = \exp\left[-\frac{(x - x_0)^2}{2\sigma_0^2}\right] \tag{3}$$

and

$$C(x, 0) = C_0, \ 0 \leqslant x \leqslant \Delta l \text{ and } C(x, 0) = 0,$$
$$x > \Delta l, \ x < 0 \tag{4}$$

where x_0 is the initial peak position, σ_0 is its initial dispersion, Δl is the initial width of the rectangular pulse and C_0 is the initial concentration in the pulse.

Assuming that the capillary is infinite, then the boundary conditions for eqn. 1 are the conditions at infinity and are given by

$$C(\pm\infty, t) = 0 \tag{5}$$

The analytical solution to eqn. 1 with the initial condition of eqn. 3 and the boundary condition of eqn. 5 is given by
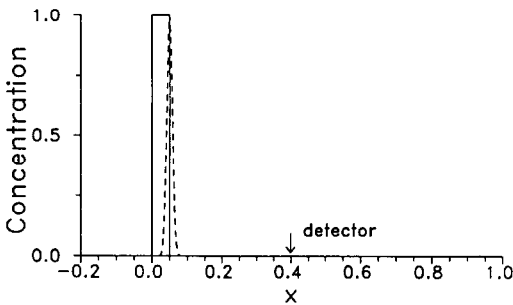

Fig. 1. Initial concentration profiles for model electrophoresis problems. The dashed line gives the profile for the linear equation ($\alpha = 0$) and the solid line gives that for the non-linear equation ($\alpha \neq 0$); detection point $x_d = 0.4$.

$$C(x_d, t) = \frac{A}{\sqrt{4\pi D(t^* + t)}} \exp\left[\frac{-(x_d - x_0 - ut)^2}{4D(t^* + t)}\right] \tag{6}$$

$$t^* = \frac{A^2}{4\pi D}, \ A = \int_{-\infty}^{+\infty} C(x, t) \, dx = \sqrt{2\pi}\sigma_0$$

where x_d is the coordinate of the detection point. Eqn. 6 gives the concentration at the detection point as a function of time.

The second type of solution for eqns. 1 and 2 in a non-diffusional, non-linear case ($\alpha \neq 0$ and $D = 0$) with the initial condition of eqn. 4 is given by

(1) $\alpha < 0$:

$$C(x_d, t) =$$

$$\left\{\begin{array}{ll} \frac{1}{\alpha}\left(1 - \sqrt{\frac{u_0 t}{x_d - \Delta l}}\right), & t_{min} < t < t_{max} \\ 0, & t < t_{min} \text{ or } t > t_{max} \end{array}\right\} \tag{7}$$

$$t_{min} = \frac{x_d - \Delta l}{u_0}$$

$$t_{max} = \frac{1}{u_0}(\sqrt{|\alpha|\Delta l \, C_0} + \sqrt{x_d - \Delta l})^2$$

(2) $\alpha > 0$:

$$C(x_d, t) =$$

$$\left\{\begin{array}{ll} \frac{1}{\alpha}\left(1 - \sqrt{\frac{u_0 t}{x_d}}\right), & t_{min} < t < t_{max} \\ 0, & t < t_{min} \text{ or } t > t_{max} \end{array}\right\} \tag{8}$$

$$t_{min} = \frac{1}{u_0}(\sqrt{\alpha \, \Delta l \, C_0} - \sqrt{x_d})^2$$

$$t_{max} = x_d/u_0$$

where t_{min} and t_{max} are the moments when the zone appears and disappears at the detection point. Eqns. 7 and 8 are obtained from eqns. 10 and 14 in ref. 23, and their validity has the same limits as those of ref. 23.

The analytical solutions presented above are important for understanding diffusion (case 1) and electrochemical broadening (case 2) in zone electrophoresis. However, they describe only the

simplest possible cases and fail when applied, e.g., to the case when both electrochemical and diffusion broadening are significant. The way to simulate complex behavior is to apply numerical methods to the electrophoresis equations.

Numerical solutions

The process of numerical solution usually includes two major stages. During the first, it is necessary to reduce the set of PDEs, derived in terms of infinitely small increments for continuous variables, to their discrete analogues as a set of finite-difference equations. The second stage assumes the choice of a numerical method for solving the large number of linear or non-linear algebraic equations, resulting from the previous stage of discretization. The final result and the quality of numerical solution depend on both stages. However, most of the work on computer simulation of electrophoresis [3,5,9,10] in the sections devoted to numerical algorithms pay attention mainly to the second stage of a solution process. In their considerations they are restricted to the problem of numerical stability of the algorithm [3,5], its computational efficiency [5,9] or the organization of calculations [7]. However, as has been shown [13], it is also very important to analyse theoretically the stage of discretization, accounting for the specifics of the governing equations. In this paper we demonstrate how the appropriate choice of a finite-difference scheme for the mass transport equation may significantly improve the quality of a solution and, hence, fulfil simulations more efficiently and for a much wider range of experimental parameters.

The characteristic feature of electrophoresis simulations is the necessity to solve numerically the set of non-stationary mass transfer equations similar to eqn. 1, which are PDEs with a small parameter D multiplying the second derivative (indeed, it is more correct to consider as a small parameter the combination $\tilde{D} = D/UL$, where U and L are the velocity and the linear dimension scales, respectively). This is a difficult task even for problems with one space dimension because, as has been pointed out [13], one should use a finite-difference grid with very small space increments to avoid some negative effects of a purely

computational nature. These effects originate from discretization of PDEs when one replaces eqn. 1 with its discrete analogue, i.e., finite-difference scheme. Discretization includes the introduction of a finite-difference grid with space step h and time step τ instead of continuous space and time variables and projection of all functions on the nodes of the grid (for details and notation, see Appendix B). One of the crucial points here is how to approximate the convective term $\partial(uC)/\partial x$. The two simplest and most commonly used approaches are the "upwind" difference and central difference approximations. The approximation with "upwind" difference gives the finite-difference scheme with an approximation error proportional to the first power of space step h [25]. The effects of numerical diffusion, which often is much greater than the physical diffusion (especially for small $\tilde{D}$), is inherent in such schemes. This numerical diffusion could entirely obscure the physical results, which has been demonstrated for ITP separations [13]. The finite-difference schemes used by most workers [3,5,9,10] approximate the convective term by a central difference, having an error of approximation proportional to the second order of h. These schemes are free from numerical diffusion, but they give spurious oscillations in the regions with sharp gradients if the space step h in a finite-difference grid is not small enough. It has been shown [13] that the oscillations are associated with the dispersion, introduced by the discretization.

The origin of these two non-physical effects (numerical diffusion and numerical dispersion) lies in the discretization stage, so they cannot be eliminated in the stage of solution of finite-difference equations. Theoretically, to reduce their negative influence, it is necessary to use a finite-difference grid with space steps h much less than $\tilde{D}$, but in practice it is often sufficient to use $h \sim \tilde{D}$. However, for very small $\tilde{D}$ values this restriction on h becomes too severe. In order to overcome it, a special finite-difference scheme with artificial dispersion was developed for electrophoresis problems [13]. It allows one to solve eqn. 1 accurately using the finite-difference grid with $h \sim \sqrt{\tilde{D}}$, which considerably reduces the calculation effort.

270

S.V. Ermakov et al. / J. Chromatogr. A 661 (1994) 265–278

In our simulations we compare three basic finite-difference algorithms. In the first, similar to those used by others [3,9,10], the convective term is approximated in eqn. 1 by a central difference equation and the diffusive term with the usual three-point equation. In the second algorithm [1,5], the convective term is approximated as in the previous case, but the diffusive term is replaced with a five-point equation. The third algorithm implements the finite-difference scheme with artificial dispersion as reported in ref. 13. All these algorithms are described in Appendix B and denoted as B1, B2 and B3, respectively. As mentioned above, the numerical algorithm is determined by (i) the stage of discretization and, particularly, the space discretization, and (ii) the solution method for ordinary differential equations resulting from space discretization or, if the temporal discretization leads to a set of algebraic equations, the solutions method for algebraic equations. As it was difficult to establish exactly what method was used in previous work [3,5,7,9,10], we chose the Euler method for integration of the set of ordinary differential equations with temporal derivative (finite-difference scheme B1) and the Runge–Kutta method for integration of the set of ordinary differential equations with temporal derivative (algorithm B2). The set of linear equations resulting from discretization by the finite-difference scheme B3 was solved by the Gauss exclusion algorithm. In this paper we do not compare these calculation methods, as our aim was to study the advantages of finite-difference schemes. Therefore, the results presented here reflect the quality of a finite-difference scheme, or more exactly its space discretization. It should be pointed out that the algorithms considered differ only in this respect. All other parts, including the solution of the non-linear algebraic equation of electroneutrality, were the same in all three.

The properties of the three algorithms were compared by solving model electrophoresis problems described above, which admit exact analytical solutions. They were also applied to simulation of two-component sample separations by means of CZE and ITP.

EQUIPMENT

All calculations were performed on an IBM PS/2 Model 70 386 computer. Computer programs were written in Microsoft FORTRAN Version 5.1. Figures were drawn by using GRAPHER (Golden Software).

RESULTS AND DISCUSSION

During the first series of simulations, three finite-difference schemes, B1, B2 and B3, were applied to eqn. 1 governing translation and diffusion of an initial pulse (eqn. 3) along the x-axis with a constant dimensionless velocity $u_0 = 1$. Three dimensionless diffusion coefficients were used for simulations: $\tilde{D} = 2 \cdot 10^{-5}$, $\tilde{D} = 1 \cdot 10^{-4}$ and $\tilde{D} = 1 \cdot 10^{-3}$. The first case might correspond to the electrophoretic run of a sample with a diffusion coefficient of $2 \cdot 10^{-5}$ cm^2 s^{-1} in a capillary of length 50 cm and a migration time from end to end of 42 min. The second case corresponds to a five times longer migration time of the same sample, *i.e.*, *ca.* 3.5 h. The detection point was at $x_d = 0.4$. The initial distribution of concentration was given by a Gaussian peak (eqn. 3), positioned at $x_0 = 0.05$ and having unit height and mass $A = 0.02$. All simulations were performed with the spatial increments being equal to $h = 2 \cdot 10^{-3}$. Temporal increments were found from the condition of stability and were equal to $\tau = 1 \cdot 10^{-3}$ for schemes B2 and B3 and $\tau = 1 \cdot 10^{-4}$ for scheme B1. The data on space and time increments on this and all subsequent simulations are summarized in Table I.

Figs. 2 and 3 compare the three numerical results with the exact analytical solution (eqn. 6) for the two diffusion coefficients $\tilde{D} = 2 \cdot 10^{-5}$ and $\tilde{D} = 1 \cdot 10^{-4}$, respectively. The numerical electropherograms are shown by solid lines and the analytical solutions by dashed lines. For the first case, Fig. 2A and B show large-amplitude oscillations of numerical electropherograms, obtained by algorithms B1 and B2, whereas scheme B3 gives a non-oscillating solution (Fig. 2C) that agrees well with the exact analytical solution. In both instances $\tilde{D} \ll h$, but $h \geqslant \sqrt{\tilde{D}}$. In addition to the absence of oscillations, another advantage

TABLE I

FINITE-DIFFERENCE GRID PARAMETERS USED FOR CALCULATIONS

The space increment in all simulations was $h = 2 \cdot 10^{-3}$.

Algorithm	Time step, τ	Parameter $\tilde{D}$	Parameter α or separation technique	Fig.
B1	10^{-4}			2A
B2	10^{-3}	$2 \cdot 10^{-5}$	0	2B
B3	10^{-3}			2C
B1	10^{-4}			3A
B2	10^{-3}	$1 \cdot 10^{-4}$	0	3B
B3	10^{-3}			3C
B1	$5 \cdot 10^{-5}$			4A
B2	10^{-3}	$2 \cdot 10^{-5}$	-0.5	4B
B3	10^{-3}			4C
B1	10^{-5}			5A
B2	10^{-4}	$1 \cdot 10^{-4}$	0.3	5B
B3	$5 \cdot 10^{-4}$			5C
B1	$5 \cdot 10^{-5}$			6A
B2	$2.5 \cdot 10^{-4}$	$(1.46–2.52) \cdot 10^{-3}$	ITP	6B
B3	$2.5 \cdot 10^{-4}$			6C
B1	Unstable			–
B2	$2.5 \cdot 10^{-4}$	$(3.65–6.3) \cdot 10^{-4}$	ITP	7A
B3	$2.5 \cdot 10^{-4}$			7B
B1	Unstable			–
B2	Unstable			–
B3	$2.5 \cdot 10^{-4}$	$(1.46–2.52) \cdot 10^{-5}$	ITP	–
B1	$5 \cdot 10^{-5}$			8A
B2	$2 \cdot 10^{-3}$	$(2.93–5.16) \cdot 10^{-5}$	CZE	8B
B3	$2 \cdot 10^{-3}$			8C
B1	Unstable			–
B2	$2 \cdot 10^{-3}$	$(2.93–5.16) \cdot 10^{-6}$	CZE	9A
B3	$2 \cdot 10^{-3}$			9B

of the numerical solution given by scheme B3 is that it gives the least error in the peak position and the peak width. Fig. 3 shows that for higher diffusion coefficients the numerical oscillations become smaller. Nevertheless, algorithms B1 and B2 still produce numerical oscillations and asymmetric peaks, although the discrepancy between the analytical and numerical solutions is much less than in Fig. 2. For larger diffusion coefficients, the deviations of numerical solutions from the analytical solution become less and for

$D = 1 \cdot 10^{-3}$, when $\tilde{D} \approx h$, all three algorithms give excellent agreement with the analytical solution. However, this value of the dimensionless diffusion coefficient corresponds to a migration time of ca. 35 h and can hardly be considered as realistic.

Figs. 4 and 5 give examples of the calculation of an electrophoresis run by using the three finite-difference algorithms, when a sample interacts with the background electrolyte, $\alpha \neq 0$ and the velocity is not constant. The initial condition
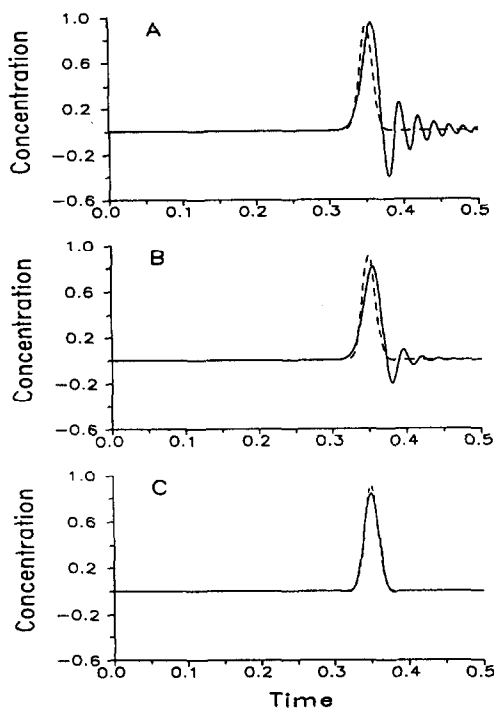
Fig. 2. Electropherograms for linear equation ($\alpha = 0$) calculated by three different finite-difference algorithms. Dimensionless diffusion coefficient $\tilde{D} = 2 \cdot 10^{-5}$. Here and also in Figs. 3–5 simulated results are plotted as solid lines and analytical results as dashed lines. Panels A, B and C represent the results obtained using finite-difference algorithms B1, B2 and B3, respectively. Concentration and time are measured in units of the maximal initial concentration and total migration time (L/u_0), respectively, with L being the length of the capillary.
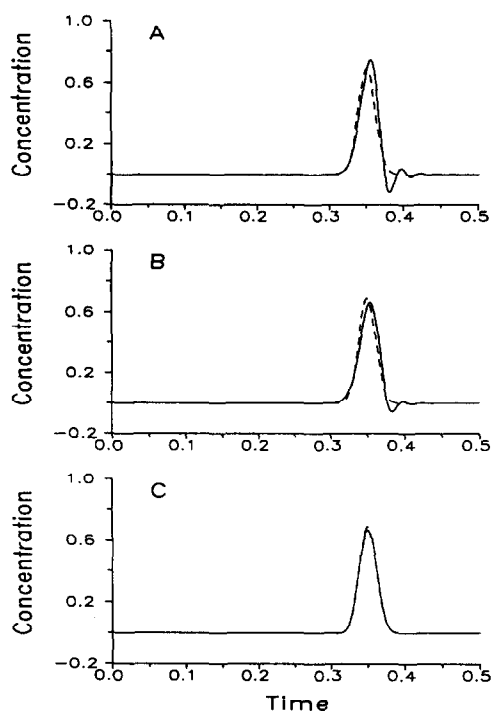

Fig. 3. Electropherograms for linear equation ($\alpha = 0$). Dimensionless diffusion coefficient $\tilde{D} = 1 \cdot 10^{-4}$. Other details as in Fig. 2.

was a rectangular pulse (see Fig. 1) of unit height and width equal to 0.05 starting at $x = 0$. Numerical results are compared in Fig. 4 for $\alpha = -0.5$ and in Fig. 5 for $\alpha = 0.3$ with analytical diffusionless solutions given by eqns. 7 and 8. As all three numerical schemes need a finite value of the diffusion coefficient, the relatively low values of $D = 2 \cdot 10^{-5}$ for $\alpha = -0.5$ and $D = 1 \cdot 10^{-4}$ for $\alpha = 0.3$ were chosen for all schemes. The detection point was at $x_d = 0.4$, $u_0 = 1$. The space increment was the same in all three instances, but temporal increments varied so as to provide stability of calculations. It is seen from Figs. 4 and 5 that for both $\alpha < 0$ and $\alpha > 0$ only the scheme with artificial dispersion (B3) is able to calculate electropherograms close to the exact analytical solution, whereas algorithms B1 and

B2 give solutions with spurious large-amplitude oscillations behind the concentration jump in the profile. Calculations with a smaller time increment τ do not lead to improvements in numerical solutions because, as stated in Theory section, they result from an improper space discretization. The diffusion effects, as seen from Figs. 4C and 5C, are small, so that the comparison of the numerical solution with $\tilde{D} \neq 0$ and the analytical solution for $\tilde{D} = 0$ can be considered as correct. In these simulations the correlation between parameters $\tilde{D}$ and h, the finite-difference algorithms and the shapes of concentration profiles, obtained using these schemes, is similar to that in the previous simulations.

In the following example, two series of simulations were applied to CZE and ITP separations for a two-component sample composed of the weak bases aniline and pyridine. It was necessary to investigate the behaviour of different numerical algorithms for conditions close to those in real experimental runs. For this purpose, simula-
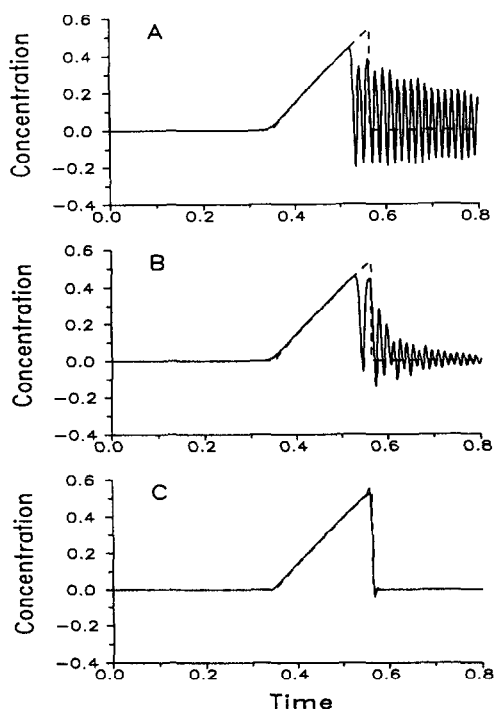
Fig. 4. Electropherograms for non-linear equation ($\alpha = -0.5$). Dimensionless diffusion coefficient $\tilde{D} = 2 \cdot 10^{-5}$. Other details as in Fig. 2.

Fig. 5. Electropherograms for non-linear equation ($\alpha = 0.3$). Dimensionless diffusion coefficient $\tilde{D} = 1 \cdot 10^{-4}$. Other details as in Fig. 2.

tions were performed at several constant but different values of applied current, approaching separation times with reasonable values. The mathematical model used in the simulations was based on the same assumptions as stated in ref. 14. The set of equations is presented in Appendix A and it was solved by using the three calculation algorithms as described above. All simulations assumed a capillary of 50 μm I.D. thermostated at 25°C and with the detector located at a point with coordinate $x_d = 10$ cm. The volumes of injected samples were 20 nl for ITP runs and 10 nl for CZE runs. The lengths of the initial sample plugs corresponding to these volumes were ca. 1 and 0.5 cm, respectively. In the ITP simulation, the sample was placed in the capillary between $x_l = 1$ cm and $x_r = 2$ cm, whereas for CZE it was located within the interval $x_l = 0.5$ cm and $x_r = 1$ cm, so that the migration path to the detector in the former instance was 8 cm and in the latter 9 cm.

In the series of ITP simulations the leading electrolyte was composed of 18 mM sodium hy-
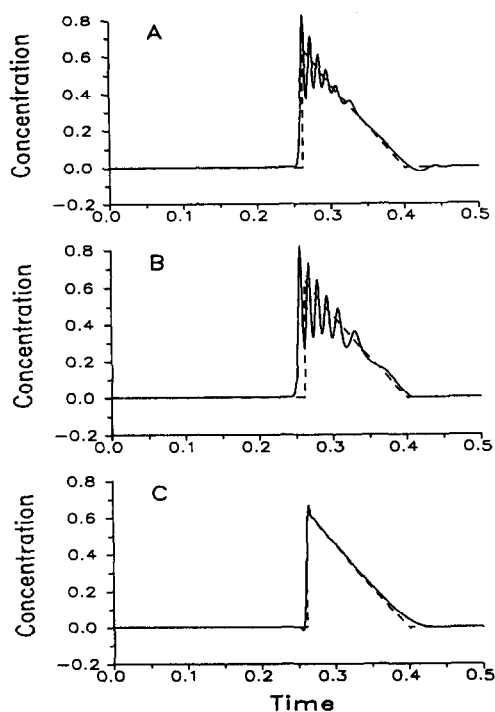
droxide and 20 mM acetic acid, which was the common counter ion in the system, the terminating electrolyte being 40 mM β-alanine plus 50 mM acetic acid. In the sample zone the initial concentrations were 10 mM aniline, 10 mM pyridine and 20 mM acetic acid. The data on ionic mobilities and pK values for specified substances used in the simulations are presented in Table II.

TABLE II

INPUT DATA FOR COMPUTER SIMULATIONS

Substance	pK_a	$\mu(10^{-8}$ m^2/V·s)
Tris	8.3	2.41
β-Alanine	3.3	3.6
Pyridine	5.18	3.0
Aniline	4.8	3.25
Acetate	4.75	4.24
Na$^+$	–	5.19
H$^+$	–	36.3
OH$^-$	–	20.5

Simulations were performed for four values of applied current, 0.05, 0.2, 0.5 and 5 μA.

As in previous simulations, the results are presented in the form of detector signals measured separately for each substance. For a current value of $J = 0.05$ μA, the concentration profiles are depicted in Fig. 6, where A, B and C show the simulation data obtained with finite-difference algorithms B1, B2 and B3, respectively. In order to provide computational stability, the temporal increment τ for algorithm B1 was chosen to be five times smaller than the increments used in the other two algorithms (see Table I). The dimensionless parameter $\tilde{D}$ here
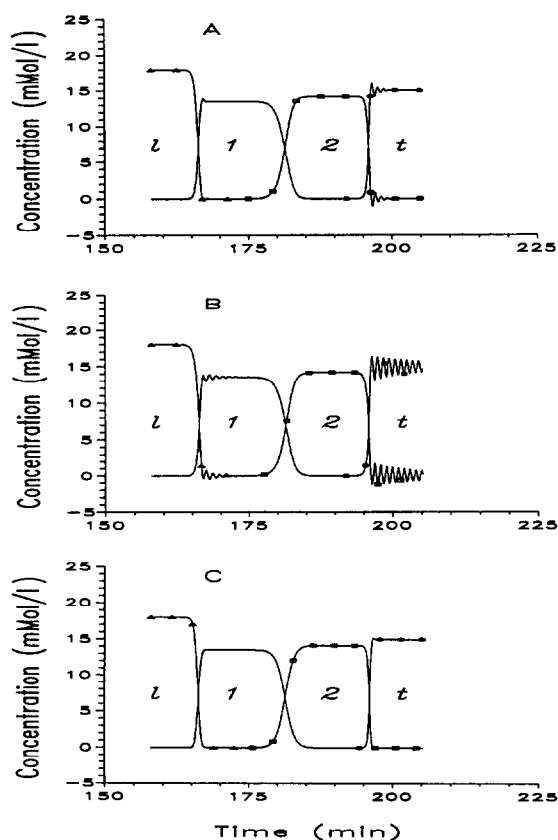

Fig. 6. Simulation for ITP separation of aniline and pyridine. Current, 0.05 μA. Panels A, B and C represent the results obtained using finite-difference algorithms B1, B2 and B3, respectively. Here and also in Fig. 7 pure zones of leader, substance components pyridine and aniline and terminator are designated by l, 1, 2 and t, respectively. ▲ = Sodium hydroxide (leader); line without symbols = pyridine (component 1); □ = aniline (component 2); ● = β-alanine (terminator).

lies within the range $1.46 \cdot 10^{-3} \leqslant \tilde{D} \leqslant 2.52 \cdot 10^{-3}$ and have the order of magnitude of the space increment $h(\tilde{D} \approx h$, see Table I). Fig. 6 shows that only the solution given by finite-different scheme B3 is free from spurious oscillations. Conversely, the concentration profiles obtained by schemes B1 and B2 contain substantial oscillations in the regions close to the zone boundaries. The amplitude and the number of oscillations depend on the magnitude of the concentration gradients. For example, at the interface between sample species 1 and 2 the gradients are smaller than at the other interfaces and no oscillations are observed here. In contrast, the oscillations have the greatest amplitude at the 2–T interface (Fig. 6A and B), where the self-sharpening effect is the strongest and concentrations are changing most sharply. Nevertheless, these two solutions may be considered to be feasible, as they allow one to obtain valuable information on separation times and concentration distributions.

However, this simulation was performed for small current values, so that the migration path of barely 8–9 cm took between 2 and 3 h, which would be unsatisfactory in real experiment. The next example was simulated for a current four times greater, i.e., $J = 0.2$ μA, and the results are shown in Fig. 7, obtained with algorithms (A) B2 and (B) B3 only; attempts to perform simulations with algorithm B1 demanded too much computational effort because, in order to provide the necessary computational stability one would have to use very small time increments. The concentration profiles calculated with algorithm B2 are severely distorted by false oscillations, which obscure the separation pattern. The solution given by B3 demonstrates only small spikes just near the zone interfaces. The other feature observed in Fig. 7 is the different lengths of zone 2 in A and B. According to Fig. 7A, the terminating electrolyte reaches the detector by $t = 48$ min, whereas in Fig. 7B this time is 49 min. The last value is correct as it corresponds to the value obtained in the previous simulation (Fig. 6) divided by four (the electric current is four times greater and, therefore, the migration time must be exactly four times less).
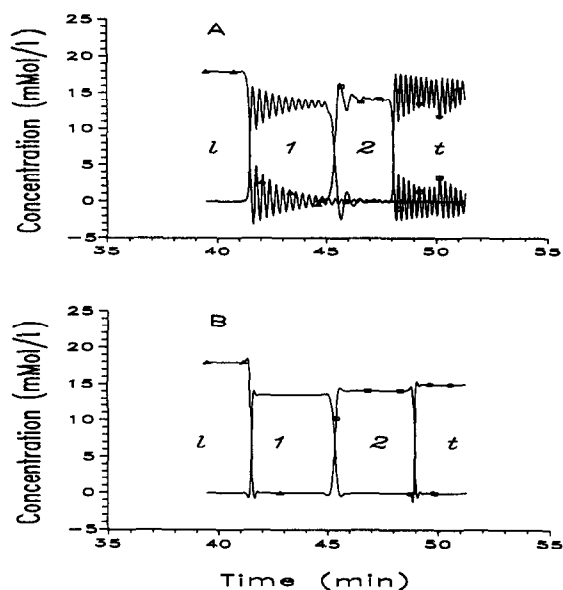
Fig. 7. Simulation for ITP separation of aniline and pyridine. Current, 0.2 μA. Panels A and B represent the results obtained using finite-difference algorithms B2 and B3, respectively. Other details as in Fig. 6.

Fig. 8. Simulation for CZE separation of aniline and pyridine. Current, 1 μA. The first substance detected is pyridine (left zone, between 20 and 30 min) and the second is aniline (right zone, between 30 and 40 min). Panels A, B and C represent the results obtained using finite-difference algorithms B1, B2 and B3, respectively.

The simulations at greater current values, $J =$ 0.5 and 5 μA, could be performed only by using algorithm B3, as the other two exhibit computational instability. For these currents the solution given by B3 was slightly distorted by spikes analogous to those in Fig. 7B. However, their amplitude was smaller than that of the oscillations in Fig. 7A, and the zone length was resolved correctly.

In the next series of simulations, modelling of a CZE separation of aniline and pyridine, Tris-acetate buffer was used with concentrations of Tris = 12 mM and acetic acid = 20 mM. This mixture gives a buffer with pH $\approx$ 5, which is approximately half way between the pK values of aniline and pyridine and thus provides the most suitable separation conditions. The concentration of both sample species was 1 mM. The simulations were performed for current values $J = 1$ and 10 μA.

Concentration profiles for $J = 1$ μA calculated using the three algorithms B1, B2 and B3 are plotted in Fig. 8A, B and C, respectively. As in the previous cases, satisfactory results are obtained only with the algorithm using the finite-difference scheme B3. The other two give con-
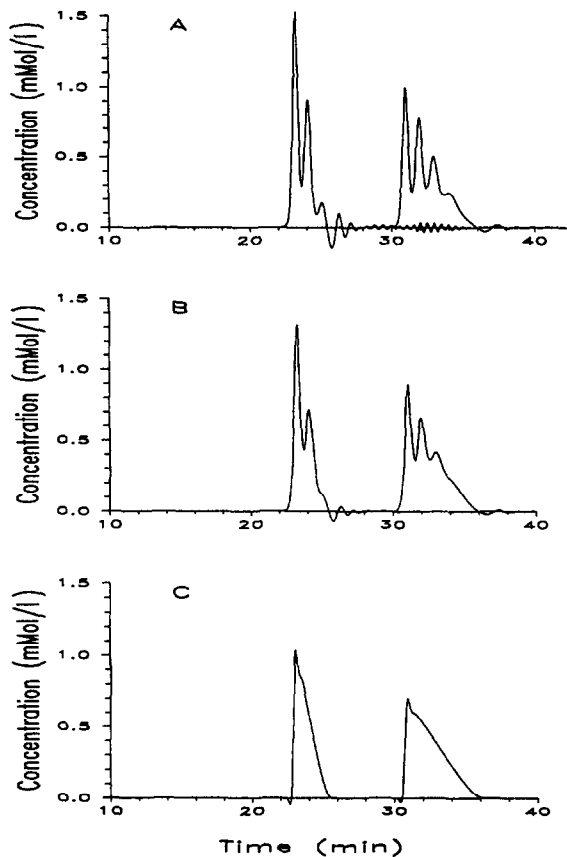
centration profiles distorted by large-amplitude oscillations and contain several peaks that could cause confusion. The positions of the first peak in Fig. 8A and B are close to the position of that in Fig. 8C, but the corresponding concentration values are different. In Fig. 8A and B they are unrealistic, as they exceed 1 mM. The profiles in Fig. 8C contain only small spikes just before and after the concentration jump. For larger currents ($J = 10$ μA, Fig. 9), the calculations by algorithm B1 were unstable up to time increments $\tau \geqslant$ 10^{-5}, so the simulation run required too much time to be performed. Scheme B2 gave a solution totally distorted by oscillations (Fig. 9A). Indeed, the separated zones decay into several
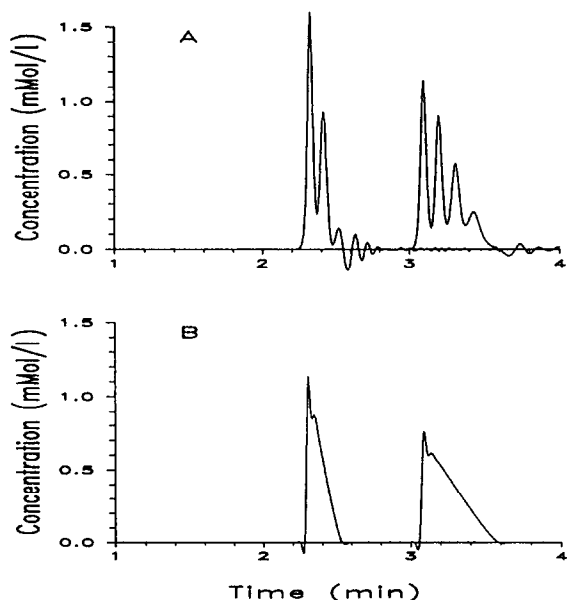
Fig. 9. Simulation for CZE separation of aniline and pyridine. Current, 10 μA. The first substance detected is pyridine (left zone, between 2 and 3 min) and the second is aniline (right zone, between 3 and 4 min). Panels A and B represent the results obtained using finite-difference algorithms B2 and B3, respectively.

solitary waves (solitons), resulting from the action of numerical dispersion [11]. The concentration profiles obtained by algorithm B3 (Fig. 9B) still retain the correct shape, but the non-physical spikes become greater.

CONCLUSIONS

Computer science is today applied with increasing frequency to the solution of problems in separation science. This is welcome in the field of electrokinetic processes, owing to the great complexity and non-linearity of electrophoresis equations. Thus, the efforts undertaken years ago by Bier's group at the Center for Separation Science in Tucson, AZ [5,6], by Dose and Guiochon [3], by Gaš and co-workers [9,10] and by Fidler et al. [7,8] represent an important step in the right direction, because in principle they should allow the experimenter to predict and optimize the separation by a "dry chemistry" approach (i.e., by computer simulations) prior to the "wet chemistry" run. Unfortunately, so far none of these approaches has found its way into

laboratory practice (except perhaps in the few laboratories which have developed such programs), so they have been of no utility to most of the potential users. As it turns out from this study, this is not because such programs have not been offered on the market, but rather because they were unable to predict real experimental conditions. Previously reported algorithms could only be adopted for solving separations at unrealistically low current densities, in general two to three orders of magnitude lower than those generally utilized in routine practice. Under these conditions, the transit times of analytes would be of the order of one to two days of electrophoresis, which does not compare favourably with modern electrophoretic science, where analyte peaks (especially in CZE) could be swept past the detector in a few minutes. When these algorithms were tried by us at real current densities, all of them broke down in a nightmare of numerical oscillations, which bore no resemblance to reality. We therefore feel that the solutions proposed and adopted here, which can still predict the correct peak shape and structure under real experimental conditions, could be an important step forward in computer science as applied to electrophoresis and facilitate the approach of newcomers to this important field of separation science. In conclusion, we believe that computer science applied to separation processes will grow more and more in importance and will soon become the basis on which to build any type of separation.
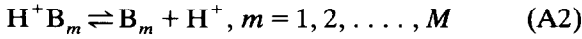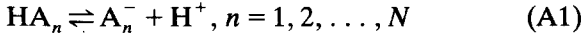
APPENDIX A

Governing equations

Our mathematical model is based on assumptions formulated in refs. 1 and 14.

An aqueous solution contains weak monoval-

ent acids HA_n and bases B_m, for which the association–dissociation reactions can be represented by

$$HA_n \rightleftharpoons A_n^- + H^+, n = 1, 2, \ldots, N \quad \text{(A1)}$$

$$H^+B_m \rightleftharpoons B_m + H^+, m = 1, 2, \ldots, M \quad \text{(A2)}$$

$$H_2O \rightleftharpoons H^+ + OH^- \quad \text{(A3)}$$

Dissociation equilibrium constants K_n^a and K_m^b and degrees of dissociation α_n and β_m are given by

$$K_n^a = \frac{[A_n^-][H^+]}{[HA_n]}, \quad \alpha_n = \frac{K_n^a}{K_n^a + [H^+]},$$
$$n = 1, 2, \ldots, N \quad \text{(A4)}$$

$$K_m^b = \frac{[B_m][H^+]}{[H^+B_m]}, \quad \beta_m = \frac{[H^+]}{K_m^b + [H^+]},$$
$$m = 1, 2, \ldots, M \quad \text{(A5)}$$

$$[H^+][OH^-] = K_w \quad \text{(A6)}$$

where $K_w = 10^{-14}$ is the ionic product of water.

The analytical concentrations of acids, $a_n = [HA_n] + [A_n^-]$, and bases, $b_m = [B_m] + [H^+B_m]$, obey the mass conservation laws:

$$\frac{\partial a_n}{\partial t} + \nabla(z_n^a \alpha_n \mu_n^a a_n \vec{E} - D_n^a \nabla a_n) = 0, \ z_n^a = -1,$$
$$n = 1, 2, \ldots, N \quad \text{(A7)}$$

$$\frac{\partial b_m}{\partial t} + \nabla(z_m^b \beta_m \mu_m^b b_m \vec{E} - D_m^b \nabla b_m) = 0,$$
$$z_m^b = +1, \ m = 1, 2, \ldots, M \quad \text{(A8)}$$

where μ_n^a and μ_m^b are the ionic mobilites and D_n^a and D_m^b are the diffusion coefficients for acids (a) and bases (b), which are expressed by the Einstein equation:

$$D = RT\mu/F$$

where $F = 96\,484$ C/mol is the Faraday constant, T is the absolute temperature and R = 8.314 J/mol·K is the universal gas constant.

The continuity equation for an electric current has the form

$$\nabla \cdot \vec{j} = 0 \quad \text{(A9)}$$

The generalized Ohm's law is given by

$$\vec{j} = F\left\{ \left(\sum_n (z_n^a)^2 \alpha_n \mu_n^a a_n + \sum_m (z_m^b)^2 \beta_m \mu_m^b b_m \right. \right.$$
$$\left. + \mu_H[H^+] + \mu_{OH}[OH^-] \right) \cdot \vec{E} - \sum_n z_n^a D_n^a \nabla(\alpha_n a_n)$$
$$- \sum_m z_m^b D_m^b \nabla(\beta_m b_m) - D_H \nabla[H^+]$$
$$\left. + D_{OH} \nabla[OH^-] \right\} \quad \text{(A10)}$$

The electroneutrality equation is valid:

$$q = F\left(\sum_m z_m^b \beta_m b_m + [H^+] + \sum_n z_n^a \alpha_n a_n - [OH^-] \right)$$
$$= 0 \quad \text{(A11)}$$

APPENDIX B

We introduce the finite-difference grid Ω by dividing the calculation interval $[0, L]$ into I equal subintervals (space steps) $h = L/I$, and by dividing the time interval $[0, T]$ into K equal time subintervals (time steps) $\tau = T/K$, i.e., $\Omega = \{x_i = (i-1) \cdot h, i = 1, 2, \ldots, I + 1,\} \times \{t^k = k \cdot \tau, k = 1, 2, \ldots, K + 1\}$.

The following notation is introduced:

$$f_i^k = f(x_i, t^k) = f_i, \quad f_i^{k+1} = f(x_i, t^{k+1}) = \hat{f}_i,$$

$$f_i^{(0.5)} = \frac{1}{2}(\hat{f}_i + f_i), \quad f_{i+1/2}^k = \frac{1}{2}(f_{i+1}^k + f_i^k)$$

where $f = f(x, t)$ is an arbitrary function.

For the finite-difference approximation of derivatives we use the notation

$$f_t = \frac{\hat{f}_i - f_i}{\tau}, \quad f_x = \frac{f_{i+1} - f_i}{h}, \quad f_{\bar{x}} = \frac{f_i - f_{i-1}}{h},$$

$$f_{\dot{x}} = \frac{f_{i+1/2} - f_{i-1/2}}{h}, \quad f_{\dot{x}} = \frac{f_{i+1} - f_{i-1}}{2h},$$

$$f_{x\bar{x}} = \frac{f_{i+1} - 2f_i + f_{i-1}}{h^2},$$

$$f_{\bar{x}x\bar{x}} = \frac{f_{i+1} - 3f_i + 3f_{i-1} - f_{i-2}}{h^3},$$

$$f_{x\bar{x}x} = \frac{f_{i+2} - 3f_{i+1} + 3f_i - f_{i-1}}{h^3}$$

In the text we refer to $f_{\bar{x}}$ and $f_{\hat{x}}$ as the "upwind" and "central" differences, respectively.

The first algorithm we consider uses the Euler integration method for the set of ordinary differential equations resulting from the space discretization. It is written at every space grid node as

$$C_t + (uC)_{\hat{x}} - D \cdot C_{x\bar{x}} = 0 \qquad (B1)$$

In the second algorithm we have the set of ordinary differential equations, written at every x_i node:

$$\frac{dC}{dt} + (uC)_{\hat{x}} - D \cdot (C_{\hat{x}})_{\hat{x}} = 0 \qquad (B2)$$

which are integrated using the Runge–Kutta method [26].

The finite-difference scheme underlying the third algorithm in the above notation has the form

$$C_t + (uC^{(0.5)})_{\hat{x}} - D \cdot C_{x\bar{x}}^{(0.5)} + \mathscr{A} + \mathscr{B} + \mathscr{C} = 0$$

$$(B3)$$

where

$$\mathscr{A} = -\frac{h^2}{6}[\text{sign}(u) \cdot (uC^{(0.5)})_{\bar{x}x\bar{x}}$$

$$+ (1 - \text{sign}(u)) \cdot (uC^{(0.5)})_{x\hat{x}x}]$$

$$\mathscr{B} = \frac{h^2}{4}(u_x C_x^{(0.5)})_{\hat{x}}$$

$$\mathscr{C} = \frac{\tau^2}{12h}[u_{i+1/2}(u \cdot C_t)_x - u_{i-1/2}(u \cdot C_t)_{\bar{x}}]$$

$$\text{sign}(u) = 1 \text{ if } u > 0$$

$$\text{sign}(u) = 0 \text{ if } u \leqslant 0$$

The finite-difference scheme B3, in addition to three common terms contained in all the schemes, also has three additional terms, $\mathscr{A}$, $\mathscr{B}$ and $\mathscr{C}$, responsible for artificial dispersion [13]. The terms $\mathscr{A}$ and the $\mathscr{C}$ were used for all simulations, whereas $\mathscr{B}$ was set to zero in simulations of CZE and ITP.

REFERENCES

1 R.A. Mosher, D.A. Saville and W. Thormann, *The Dynamics of Electrophoresis*, VCH, Weinheim, 1992.

2 D. Tietz, *Electrophoresis*, 13 (1992) 339.

3 E.V. Dose and G.A. Guiochon, *Anal. Chem.*, 63 (1991) 1063–1072.

4 R.A. Mosher, P. Gebauer, J. Caslavska and W. Thormann, *Anal. Chem.*, 64 (1992) 2991–2997.

5 O.A. Palusinski, A. Graham, R.A. Mosher, M. Bier and D.A. Saville, *AIChE J.*, 32 (1986) 215–223.

6 R.A. Mosher, D. Dewey, W. Thormann, D.A. Saville and M. Bier, *Anal. Chem.*, 61 (1989) 362–366.

7 V. Fidler, J. Vacík and Z. Fidler, *J. Chromatogr.*, 320 (1985) 167–174.

8 Z. Fidler, V. Fidler and J. Vacík, *J. Chromatogr.*, 320 (1985) 175–183.

9 B. Gaš, J. Vacík and I. Zelenský, *J. Chromatogr.*, 545 (1991) 225–237.

10 E. Durovčáková, B. Gaš, J. Vacík and E. Smolková-Keulemansová, *J. Chromatogr.*, 623 (1992) 337–344.

11 S.I. Muhin, S.B. Popov and Yu.P. Popov, *Zh. Vychisl. Mat. Mat. Fiz.*, 23 (1983) 1355–1369.

12 S.V. Ermakov, O.S. Mazhorova and Yu.P. Popov, Preprint of Keldysh Institute of Applied Mathematics, 1990, No. 89, p. 28 (in Russian).

13 S.V. Ermakov, O.S. Mazhorova and Yu.P. Popov, *Informatica*, 3, No. 2 (1992) 173–197.

14 S.V. Ermakov, O.S. Mazhorova and M.Yu. Zhukov, *Electrophoresis*, 13 (1992) 838–848.

15 M.Yu. Zhukov, *Zh. Vychisl. Mat. Mat. Fiz.*, 24 (1984) 549–565.

16 S.V. Ermakov, O.S. Mazhorova and Yu.P. Popov, in V.S. Advuevsky (Editor), *Proceedings of the International Symposium on Hydromechanics and Heat/Mass Transfer in Microgravity, Perm–Moscow, July 1991*, Gordon and Breach, Philadelphia, PA, 1992, pp. 409–413.

17 M. Bello, S. Levine and P.G. Righetti, *J. Chromatogr. A*, 652 (1993) 329.

18 H. Nishi and S. Terabe, *Electrophoresis*, 11 (1990) 691–701.

19 M. Chiari, M. Nesi and P.G. Righetti, *J. Chromatogr. A*, 652 (1993) 31.

20 E. Giaffreda, C. Tonani and P.G. Righetti, *J. Chromatogr.*, 630 (1993) 313–327.

21 P.G. Righetti, *Immobilized pH Gradients: Theory and Methodology*, Elsevier, Amsterdam, 1990.

22 G. Hughes, S. Frutiger, N. Paquet, F. Ravier, C. Pasquali, J.C. Sanchez, R. James, J.D. Tissot, B. Bjellqvist and D.F. Hochstrasser, *Electrophoresis*, 13 (1992) 707–714.

23 F.E.P. Mikkers, F.M. Everaerts and Th.P.E.M. Verheggen, *J. Chromatogr.*, 169 (1979) 1–10.

24 V. Šustáček, F. Foret and P. Boček, *J. Chromatogr.*, 545 (1991) 239–248.

25 C.A.J. Fletcher, *Computational Techniques for Fluid Dynamics 1, Fundamental and General Techniques*, Springer, Berlin, Heidelberg, 1988.

26 L. Lapidus and J. Seinfeld, *Numerical Solutions of Ordinary Differential Equations*, Academic Press, New York, 1971.